Key Points:
- Pure atmosphere-driven "passive" and ocean-driven "active" climate responses are isolated using a novel partial coupling method
- The spatial pattern evolution of surface temperatures and ocean heat uptake is attributable to the active ocean-driven component
- The active ocean response is largely responsible for reduced effective sensitivity compared to that at equilibrium

The Active Role of the Ocean in the Temporal Evolution of Climate Sensitivity

Oluwayemi A. Garuba[1] [ID], Jian Lu[1] [ID], Fukai Liu[2] [ID], and Hansi A. Singh[1] [ID]

[1]Pacific Northwest National Laboratory, Richland, WA, USA, [2]Physical Oceanography Laboratory/CIMST, Ocean University of China and National Laboratory for Marine Science and Technology, Qinqdao, China

Abstract The temporal evolution of the effective climate sensitivity is shown to be influenced by the changing pattern of sea surface temperature (SST) and ocean heat uptake (OHU), which in turn have been attributed to ocean circulation changes. A set of novel experiments are performed to isolate the active role of the ocean by comparing a fully coupled CO_2 quadrupling community Earth System Model (CESM) simulation against a partially coupled one, where the effect of the ocean circulation change and its impact on surface fluxes are disabled. The active OHU is responsible for the reduced effective climate sensitivity and weaker surface warming response in the fully coupled simulation. The passive OHU excites qualitatively similar feedbacks to CO_2 quadrupling in a slab ocean model configuration due to the similar SST spatial pattern response in both experiments. Additionally, the nonunitary forcing efficacy of the active OHU (1.7) explains the very different net feedback parameters in the fully and partially coupled responses.

1. Introduction

Climate sensitivity is time varying, with the effective sensitivity, estimated from a nonequilibrium transient period, always smaller than the actual equilibrium sensitivity (Murphy, 1995; Senior & Mitchell, 2000; Williams et al., 2008; Winton et al., 2010). Following the linear relation:

$$N = R - \lambda \Delta T, \tag{1}$$

where N is the net top-of-atmosphere (TOA) radiative flux, R is the radiative forcing and ΔT is the global surface temperature response, and λ is the effective climate feedback parameter, and the effective climate sensitivity is ΔT, extrapolated at $N = 0$ (Gregory et al., 2004). λ is likewise always more stabilizing than the equilibrium climate feedback.

The inconstancy of the effective climate sensitivity has been interpreted as the result of a time evolving pattern of ocean heat uptake (OHU) and its efficacy (Rose et al., 2014; Rose & Rayborn, 2016; Rugenstein et al., 2016). Where the efficacy of a forcing is defined as the ratio of surface warming, it causes relative to that due to CO_2 forcing. Climate models robustly show that OHU has an efficacy greater than 1, implying it causes weaker surface warming and a smaller effective climate sensitivity (Geoffroy et al., 2013; Held et al., 2010; Winton et al., 2010, 2013). This nonunitary OHU efficacy, therefore, is, also associated with an evolving pattern of sea surface temperature (SST) and the local and global radiative feedbacks induced by it (Andrews et al., 2015; Armour et al., 2013; Haugstad et al., 2017), and ocean circulation changes have been suggested to play an important part in these patterns.

Following abrupt CO_2 increase, ocean circulation changes redistribute ocean reservoir temperature, causing a different warming pattern from that due to the passive advection by the circulation. Consequently, this redistribution causes weaker global SST warming, and deeper heat anomaly penetration into the ocean (larger ocean heat capacity), as well as changes the pattern and magnitude of OHU (Banks & Gregory, 2006; Garuba & Klinger, 2016; Gregory et al., 2016; Xie & Vallis, 2012). By modifying SST patterns and the global surface warming response, ocean redistributive processes also modify radiative feedbacks and the OHU efficacy (Andrews et al., 2015; Armour et al., 2013; Haugstad et al., 2017; Winton et al., 2013). Winton et al. (2013) demonstrated the impact of the ocean redistribution on the OHU efficacy, by comparing simulations in which ocean circulation is fixed and free to change; the efficacy of the OHU is greater than one only when the circulation is free to change but is equal to one when held fixed. Trossman et al. (2016) concluded that interactions between cloud radiative feedbacks and ocean circulation change slow global surface warming. It is not clear, however,

how much of the temporal evolution of the SST and OHU patterns, or the effective climate sensitivity, is attributable to ocean circulation changes.

In this study, we isolate the contributions of the *pure* atmosphere-driven "passive," and ocean dynamics-driven "active" responses to the time variation of the effective climate sensitivity, by separating the SST and OHU patterns, and the climate feedbacks due to each component in a fully coupled simulation. We use a novel experimental design, in which the ocean is partially coupled to the atmosphere, such that the impact of the ocean "redistributive" temperature is removed from surface heat fluxes. We compare the climate feedbacks due to the passive and active OHU components, using a slab ocean model framework. Our approach is in the spirit of the fixed-circulation experiment of Winton et al. (2013) and Trossman et al. (2016), the ocean-only passive and active OHU decomposition by Garuba and Klinger (2016), and the "added" and "redistributed" heat decomposition of Bouttes et al. (2014) and Gregory et al. (2016). The method presented here, however, isolates more precisely, the passive and active SST and OHU components, and the climate feedbacks associated with them.

2. Model and Experimental Design

We use the fully coupled and slab ocean versions of the community Earth System Model version 1.1 (CESM 1.1 and community Earth System Model-slab ocean model (CESM-SOM)). The fully coupled CESM consists of the following active components: Community Atmospheric Model version 5 (CAM5) (Neale et al., 2012), Parallel Ocean Program version 2 (POP2) (Danabasoglu et al., 2012), Community Land Model version 4 (CLM4) (Oleson et al., 2010), and the Community Ice CodE (CICE) (Hunke et al., 2010). In the CESM-SOM, the ocean model POP is replaced by a slab ocean model (SOM; see Bitz et al., 2012). The horizontal resolution used for CAM5 and CLM4 is $2.5° \times 1.9°$, with the atmospheric component having 30 vertical levels. CICE, POP, and SOM run on a nominally 1° resolution displaced pole grid (with the north pole singularity centered over Greenland); POP has 61 vertical levels.

The fully and partially coupled simulations are both branched from a 1,000 year preindustrial control run, forced by abrupt CO_2 quadrupling, and integrated for 150 years. The slab simulations use ocean heat flux convergences computed from the pre-industrial control, partially-coupled 4xCO2 or fully-coupled 4xCO2 simulations, as described in section 2.3.

2.1. Surface-Forced and Redistributive Component Decomposition

The decomposition of the ocean temperature is inspired by the coupled (Banks & Gregory, 2006; Bouttes et al., 2014; Gregory et al., 2016) and ocean-alone tracer experiments (Garuba & Klinger, 2016; Marshall et al., 2015; Xie & Vallis, 2012). The ocean temperature anomaly is decomposed based on the evolution equation for the ocean temperature response to an external forcing expressed below:

$$\frac{DT'}{Dt} = F' - v' \cdot \nabla \bar{T} \tag{2}$$

where overbars represent the control variables, primes denote anomalies from the control, and $\frac{D}{Dt} = \frac{\partial}{\partial t} + v \cdot \nabla$ (i.e, the total derivative following the ocean circulation, $v = \bar{v} + v'$). Equation (2) posits that the total ocean temperature response (T') can be thought of being forced by surface flux anomalies (F'), and the redistribution of the background mean temperature ($\bar{T}$) by the circulation change (v'). Therefore, T' can be decomposed based on these sources, into what we will call "surface-forced" (T'_{AF}) and redistributive (T'_{RF}) components (subscript "F" denotes the fully coupled temperature components) as

$$\frac{DT'_{AF}}{Dt} = F' \tag{3}$$

$$\frac{DT'_{RF}}{Dt} = -v' \cdot \nabla \bar{T} \tag{4}$$

$$T' = T'_{AF} + T'_{RF} \tag{5}$$

Note that, T'_{AF} is due to the *total* surface heat flux anomaly, while T'_{RF} is due *only* to the background temperature redistribution, through circulation change; T'_{RF}, therefore, conserves global ocean heat content. However, this decomposition in equation (5) does not completely isolate the ocean-driven component from the atmosphere-driven one, since the total surface heat flux, F', itself is partly the result of ocean circulation changes.

2.2. Passive and Active Component Decomposition

To see this, we can write the fully coupled surface heat flux change, F', conceptually as

$$F' = \alpha(T'_{atm} - T')|_s, \tag{6}$$

where T'_{atm} is the atmospheric temperature anomaly induced by CO_2 increase, T' the ocean temperature response, $|_s$ represent surface values of the variables, and α represents the strength of the surface coupling between the atmosphere and ocean. Writing the ocean surface temperature response in terms of the components $T'|_s = T'_{AF}|_s + T'_{RF}|_s$, we see that F' will be driven not only by the atmosphere, through $T'_{atm}|_s$ and the ocean passive response $T'_{AF}|_s$ but also by the ocean itself, through its redistributive temperature response $T'_{RF}|_s$. Therefore, F' includes both an atmosphere- and ocean-driven components. The inclusion of the ocean-driven component in F' represents a major drawback of prior decompositions into surface-forced and redistributive components (Banks & Gregory, 2006; Bouttes et al., 2014; Gregory et al., 2016; Marshall et al., 2015; Xie & Vallis, 2012). The ocean-driven surface heat flux component is not included in the redistributive component in equation (4); instead, it is included in the surface-forced part, through F'; hence, both components have ocean-driven changes.

A more desirable decomposition is one with *pure* atmosphere-driven passive and ocean-driven active components, in which the passive surface heat flux drives only the passive temperature, and the active one drives only the active temperature, forming a more self-consistent attribution system. The corresponding decomposition of heat fluxes and temperature, respectively are:

$$F' = F'_{passive} + F'_{active} \tag{7}$$

$$T' = T'_{passive} + T'_{active} \tag{8}$$

where $F'_{passive}$ is the passive surface heat flux component which *excludes* the impact of the ocean redistributive surface temperature, thus due solely to the CO_2 increase in the atmosphere (similar to that in the "fixed circulation" in Winton et al., 2013 and Trossman et al., 2016 or the ocean-only tracer experiments in Garuba & Klinger, 2016). F'_{active} is the active surface heat flux component, due to the impact of the ocean redistributive temperature component on surface interaction (similar to the "redistribution feedback" in Garuba & Klinger, 2016 or "redistributed heat" in Bouttes et al., 2014 and Gregory et al., 2016). $T'_{passive}$ is the passive temperature anomaly component forced *only* by $F'_{passive}$, while T'_{active} is the active temperature component forced by ocean circulation changes and F'_{active}.

Based on these definitions, we see that $T'_{passive}$ will evolve like the fully coupled surface-forced anomaly, T'_{AF} in equation (3), but driven instead by $F'_{passive}$:

$$\frac{DT'_{passive}}{Dt} = F'_{passive} \tag{9}$$

T'_{active}, on the other hand, is the difference between the fully coupled temperature anomaly (T') and $T'_{passive}$, according to (8). Therefore, its evolution is derived using equations (2) minus (9), and (7):

$$\frac{DT'_{active}}{Dt} = F'_{active} - v' \cdot \nabla \bar{T} \tag{10}$$

Through equation (10), we see that T'_{active} consists of a part owing to the fully coupled circulation change v', and a part forced by the active surface heat flux, F'_{active}. Therefore, in comparison to T'_{RF} in (4), T'_{active} includes all the effects of ocean circulation changes and is self-contained to the extent that F'_{active} itself is attributable to the ocean circulation change.

We isolate the passive surface heat flux anomaly through a novel partial coupling framework. The partially coupled simulation has the same initialization and forcing as the fully coupled one, and is *also* decomposed into surface-forced and redistributive components. However, unlike the fully coupled one, the partially coupled ocean temperature is not used to compute surface heat fluxes, though it is driven by them. The partially coupled surfaced-forced temperature component is used instead, thereby, preventing the impact of the redistributive component on the surface fluxes (Figure 1). Therefore, the partially coupled surface heat flux anomaly is only $F'_{passive}$, as defined above, while F'_{active} is the fully coupled surface heat fluxes minus partially coupled ones, according to (7).
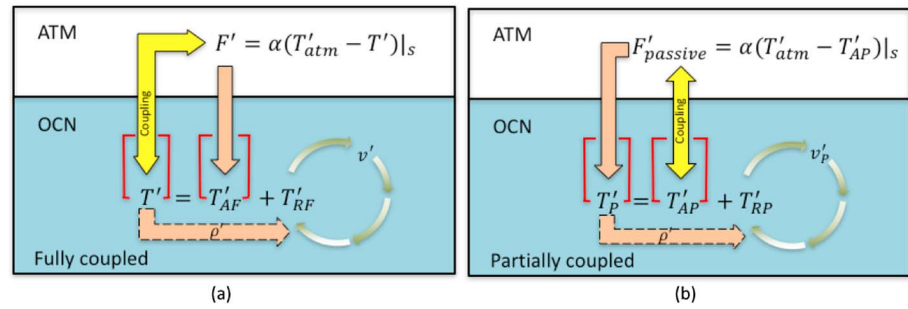
Figure 1. Surface coupling in the (a) fully coupled and (b) partially coupled simulations. The fully and partially coupled potential temperature fields (T', T'_P) are driven by the surface heat fluxes (F', $F'_{passive}$) and cause density (ρ'), and consequently, circulation changes. Their respective surface-forced (T'_{AF}, T'_{AP}) and redistributive (T'_{RF}, T'_{RP}) components are decomposed using passive tracers. The fully coupled, F', is computed using T', while the partially coupled, $F'_{passive}$, is computed using T'_{AP}. Note that the actual coupled variables include the background temperature $\bar{T}$; only anomalies are shown for simplicity.

Like their fully coupled analogs, the partially coupled surface-forced and redistributive ocean temperature components are T'_{AP} and T'_{RP} respectively (subscript "P" here denotes the partially coupled variables). T'_{AP} *is* the desired passive temperature component as defined above, since it is forced only by $F'_{passive}$; therefore, it is hereafter referred to as $T'_{passive}$. Accordingly, it evolves following equation (9), while its redistributive component evolves as:

$$\frac{DT'_{RP}}{Dt} = -v'_P \cdot \nabla \bar{T} \tag{11}$$

The partially coupled redistributive component T'_{RP}, by design is removed from coupling; therefore, it only captures the *direct* part of the active response by ocean circulation change, that is, v'_P in equation (11) (note that the fully coupled v' and the partially coupled v'_P also differ). When T'_{RP} is coupled in the fully coupled simulation, it causes not only the active surface heat flux, F'_{active}, but also additional circulation changes ($v' - v'_P$) and the redistributive temperature anomaly due to it ($T'_{RF} - T'_{RP}$), all of which are included in T'_{active} (compare equations (10) and (11)). Therefore, this uncoupled redistributive temperature offers a way to verify the validity of the derived active components, F'_{active} and T'_{active} (see discussion in section 3.1).

In practice, the decomposition of the ocean temperature anomaly into a surface-forced and redistributive components is realized through implementing two temperature tracers, formulated in the same way as in previous tracer experiments (Banks & Gregory, 2006; Garuba & Klinger, 2016; Gregory et al., 2016; Marshall et al., 2015; Xie & Vallis, 2012) (see supporting information for further details on tracer implementation). The two decomposed components add up reasonably well to the total temperature anomaly (see Figure S1).

2.3. Slab Simulations
We use slab simulations forced with the ocean mixed layer heat convergence (Q-flux) anomalies, diagnosed from the partially and fully coupled simulations, to isolate the radiative feedbacks due to the passive and active OHU components and estimate the efficacy of the active OHU component. The passive OHU slab experiment (slab$_{P-OHU}$) is forced with CO_2 quadrupling together with the Q-flux anomaly due to $T'_{passive}$, while the active OHU slab experiment (slab$_{A-OHU}$) is forced with the difference between the fully coupled Q-flux anomaly and the passive one (equivalent to the Q-flux anomaly due to T'_{active}). Note that because there is no CO_2 forcing anomaly between the fully coupled and partially coupled experiments, the slab$_{A-OHU}$ experiment is not forced with CO_2 quadrupling. These experiments are compared to a slab experiment forced with CO_2 quadrupling, and the climatological Q-flux forcing from the control slab experiment (slab$_{4xCO_2}$).

3. Results
3.1. SST and Ocean Heat Uptake Pattern
We first compare the fully coupled OHU pattern F' and its passive and active components ($F'_{passive}$ and F'_{active}, respectively), with the latter being derived from the difference between the fully and partially coupled surface fluxes ($F' - F'_{passive}$). During the first decade or so, the full OHU, F', is *relatively* uniform globally, reflecting the ocean mixed layer adjustment to CO_2-induced atmospheric warming. This feature is fully captured by the passive component of the uptake during the same period. Soon, this uniform uptake pattern is overtaken
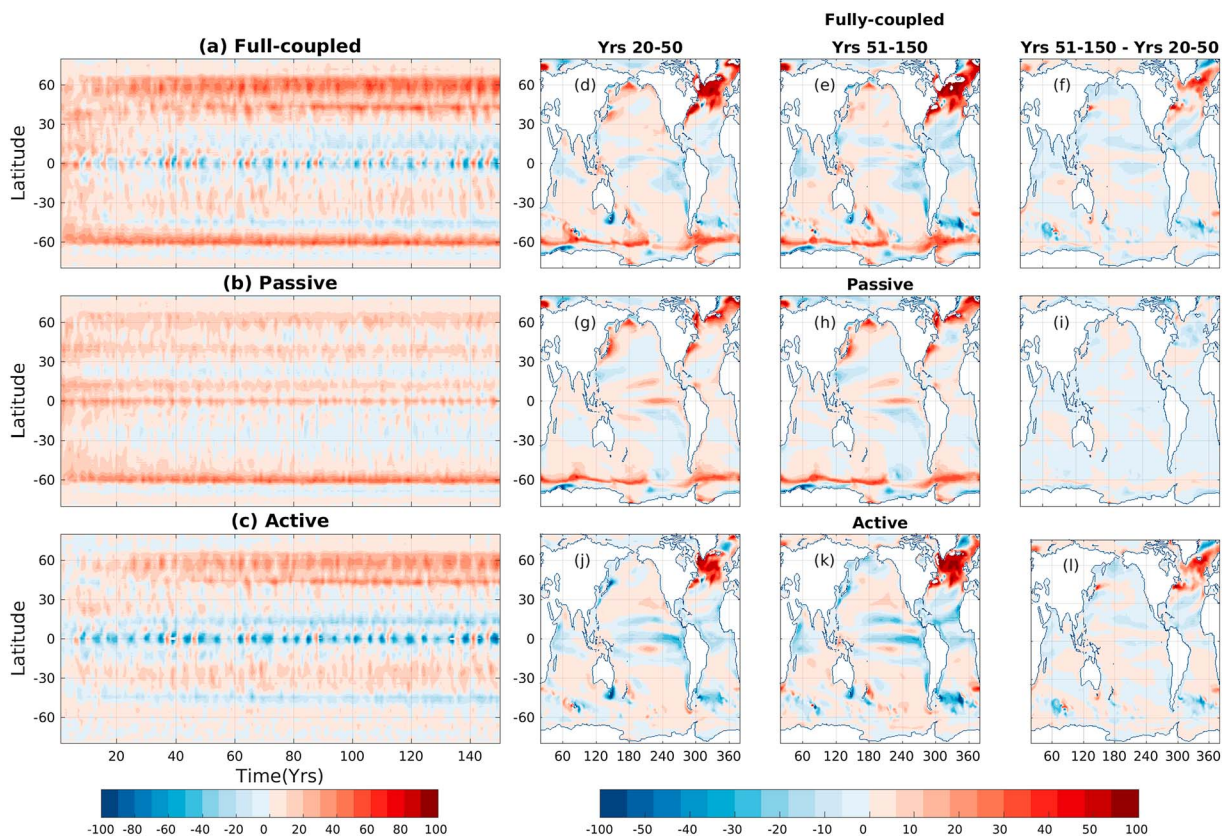
Figure 2. Zonally averaged net surface heat flux anomalies in (a) the fully coupled experiment, (b) the partially coupled experiment (passive), and (c) fully coupled minus partially coupled experiments (active). Surface heat flux anomaly evolution shown for the time mean over (d, g, and j) years 20 to 50 and (e, h, and k) years 51 to 150, and (f, i, and l) the difference between these two time periods, in the fully coupled experiment (Figures 2d–2f, respectively), in the partially coupled experiment (passive; Figures 2g–2i respectively), and the fully coupled minus partially coupled experiments (active; Figures 2j2l, respectively). Units = W m^2.

by a meridional structure with a strong subpolar uptake in both hemispheres and a heat release in the tropics. The subpolar uptake in the Southern Hemisphere (SH) is attributable largely to the passive OHU (Figure 2b), in agreement with the passive (surface-forced here) heat content decompositions of Armour et al. (2016) and Gregory et al. (2016), whereas the subpolar uptake in the Northern Hemisphere (NH) is mostly due the active OHU (i.e., resulting from the ocean circulation change; Figure 2c). The time scales for the establishment of the passive and active OHU patterns are also different: the former only takes a few decades, while the latter continues to evolve after half a century. The slow evolution of the OHU spatial pattern is examined, using the difference between the years 20 to 50 average and the 50 to 150 average (excluding the mixed layer adjustment period). Figures 2d–2f show that the slow evolution of the OHU in the fully coupled case is almost identical to that of the active OHU (Figures 2j–2l), whereas the passive OHU exhibits little change in its pattern (Figures 2g–2i). Similarly, the evolution of the fully coupled surface air temperature (SAT), and SSTs are dominated by the active components (Figures S2 and S3).

Although the passive OHU pattern is forced by the air-sea interfacial flux, its pattern is ultimately determined by the structure of the mean ocean circulation, as implied by the nature of the governing equation for tracer $T'_{passive}$. By design, $F'_{passive} = \alpha(T'_{air}|_s - T'_{passive}|_s)$, and for the slow time scale of interest, the surface air temperature ($T'_{air}|_s$ or SAT) and the passive SST component ($T'_{passive}|_s$ or $SST'_{passive}$) always follow each other closely (as also confirmed in the actual simulations). Therefore, $F'_{passive}$ is strongly shaped by $SST'_{passive}$ through the mean ocean circulation pattern. Large passive uptake occurs at upwelling regions or regions of large heat divergence due to strong ocean currents, such as at western boundaries and the equatorial Pacific. The relatively weak Southern Ocean surface warming response is caused by the deep downwelling in the Southern Ocean, as shown in Armour et al. (2016) (compare Figures 2b and 3b). The reduced ocean surface warming there creates a large air-sea temperature difference, driving the large passive uptake. Being ultimately driven
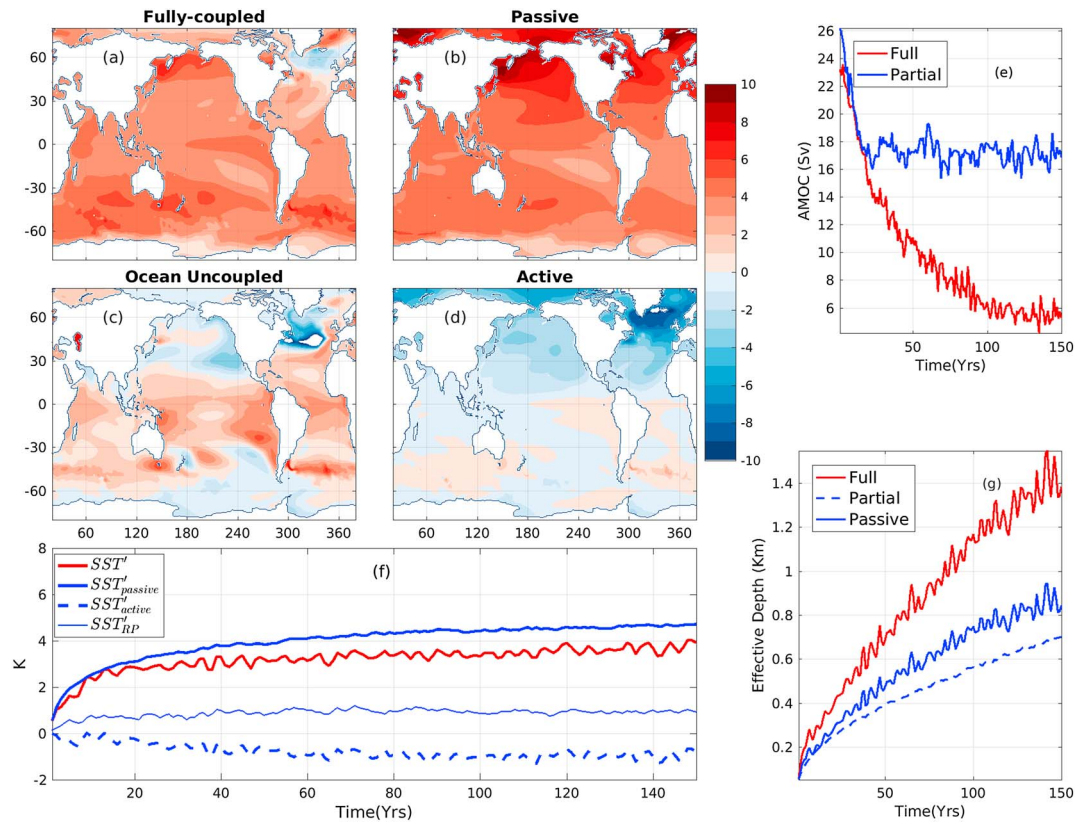
Figure 3. Fully coupled surface temperature anomaly and its components (final 50 years time mean; in K): (a) Sea Surface Temperature anomaly, SST'; (b) passive SST component (or partially coupled surface-forced, $SST'_{passive}$); (c) uncoupled redistributive component (or partially coupled SST'_{RP}); and (d) active SST component ($SST'_{active} = SST' - SST'_{passive}$). (e) Atlantic meridional overturning circulation (AMOC) index in the fully coupled (red) and partially coupled (blue) experiments. (f) Global averaged SST anomaly and its components: fully coupled SST' (red), the passive component $SST'_{passive}$ (blue solid), the active SST'_{active} (blue dashed), and the partial redistributive SST'_{RP} (thin blue solid). (g) Effective depth of uptake for the fully coupled T'(red), partially coupled T'_P (blue dashed), and passive component $T'_{passive}$ (blue).

by the advection of the mean ocean circulation, which is fixed in time, the passive OHU does not change much in time, a feature with interesting implications for the OHU efficacy (to be elaborated upon later).

The active OHU pattern (F'_{active}), on the other hand, is consistent with the uncoupled redistributive SST pattern (SST'_{RP}), inducing it (Figure 3c). A comparison of F'_{active} and SST'_{RP} reveals a strong compensating effect between them: wherever redistribution acts to warm (cool) the SST, the induced active surface heat flux works against it to cool (warm) it. Thus, showing the active tropical heat release is due to the widespread tropical warming in SST'_{RP}, while the active NH high-latitude uptake comes largely from the large Atlantic subpolar gyre cooling, caused by AMOC weakening in the partially coupled experiment (compare Figures 2c, 2j–2l, and 3c). This AMOC weakening-induced active uptake has also been shown in the studies of Winton et al. (2013), Garuba and Klinger (2016), and Gregory et al. (2016).

The derived active SST pattern (SST'_{active}) is the residual surface temperature anomaly, including the compensating effect of F'_{active} on SST'_{RP}, and additional redistributive anomalies (further circulation changes), arising from the coupling to SST'_{RP} in the fully coupled simulation (see also equations (11) and (10)). Accordingly, SST'_{active} shows much reduced warming in the tropics (El Niño-like warming) and greater cooling in the NH high latitudes, in comparison to SST'_{RP} (Figures 3c and 3d). This active Pacific El Niño-like warming pattern is shown to be a robust feature of global warming experiments in CESM, and partly due to the weakening of the shallow subtropical overturning cell (Luo et al., 2016). The widespread NH active SST cooling appears to be at odds with the large active heat uptake in the subpolar Atlantic, which would have caused anomalous warming there if acting in isolation. However, this extra NH cooling is caused by a stronger redistributive cooling effect, due to the much weaker fully coupled AMOC (Figure 3e). This additional AMOC weakening-induced

redistributive cooling can be seen by comparing the redistributive components in both simulations, SST'_{RF} and SST'_{RP} (see Figure S4).

The uncoupled surface redistributive component, SST'_{RP}, warms the ocean surface in the global average, because of the dominance of tropical warming over NH high-latitude cooling in this pattern, while the active SST component, SST'_{active}, causes a net global surface cooling, due to the widespread NH high-latitude cooling in this pattern (Figure 3f; compare also Figures 3c and 3d). Garuba and Klinger (2016) show that ocean reservoir temperature redistribution deepens the global mean depth that temperature anomalies penetrate (i.e., the effective depth of uptake), when it cools the surface, and thereby increases the magnitude of OHU and vice versa. Accordingly, the net surface cooling effect of the active SST deepens the effective depth of uptake in the fully coupled simulation compared to passive one (Figure 3g, red and blue lines), as well as the OHU magnitude (compare Figure S5).

This effective depth deepening effect, however, is a coupled effect, not an ocean-only effect as suggested in ocean-only studies (Garuba & Klinger, 2016; Xie & Vallis, 2012): as shown by the uncoupled ocean redistributive surface temperature, SST'_{RP}, the ocean by itself, causes warmer global SSTs and shallower effective depth (Figure 3g, solid and dashed blue lines); the atmospheric coupling to this ocean-only redistributive warming is what cools SSTs and deepens the effective depth (seen in SST'_{active}). The different conclusion reached in ocean-only studies might be caused by the use of fully coupled derived boundary forcings for the ocean model, which includes the coupled effect.

3.2. Climate Sensitivity and Radiative Feedbacks

Making use of equation (1), we estimate the effective climate feedback parameter, λ, as the regression coefficient in the partially and fully coupled simulations, following Gregory et al. (2004). The fully coupled simulation has a smaller effective climate sensitivity (more stabilizing λ) than the partially coupled one (Figure 4a). This reduced fully coupled effective climate sensitivity is consistent with the net cooling effect of its active ocean response (recall Figure 3f) and also suggests that the active component contributes to the time variation of the effective climate sensitivity.

Owing to the very long time the partially and fully coupled simulations will take to equilibrium, slab ocean model experiments are used to estimate equilibrium climate sensitivity, and the contributions of the passive and active components to the fully coupled effective sensitivity reduction. Slab CO_2 forcing experiments have been shown to provide a good approximation of coupled equilibrium climate sensitivity (Danabasoglu & Gent, 2009). Our $slab_{P-OHU}$ and $slab_{A-OHU}$ experiments are able to reproduce the respective passive and active SST patterns from the coupled experiments (Figure S6). Comparing the global feedbacks in the $slab_{4xCO_2}$ (λ_{CO_2}) and $slab_{P-OHU}$ (λ_{P-OHU}), which are 0.75 and 0.83, respectively, suggests that the passive OHU contributes very little to the reduced fully coupled effective climate sensitivity (enhanced effective feedback parameter) (Figure 4b). Furthermore, the effective feedback parameter of the partially coupled experiment (0.88) is not very different from its equilibrium value, approximated by that in the $slab_{P-OHU}$ (0.83). This is consistent with the stationary passive OHU pattern, and the very similar SST responses in $slab_{4xCO_2}$, $slab_{P-OHU}$, and the passive SST patterns, $SST'_{passive}$ (see Figure S6). Indeed, the meridional structure of the global feedbacks and its components in $slab_{4xCO_2}$ and $slab_{P-OHU}$ are also very similar (Figures 4c–4g, black and blue dashed lines).

Compared to the partially coupled effective feedback parameter (0.88), the fully coupled one (1.18), is significantly more stabilizing than λ_{CO_2}, (0.75), suggesting that the enhanced efficacy in the fully coupled case is largely due to the active ocean response. Using the $slab_{A-OHU}$ (where the active Q-Flux is the only forcing), we estimate the efficacy of the active OHU, defined as $\varepsilon = \lambda_{CO_2}/\lambda_{A-OHU}$ to be 1.7, which is comparable to the fully coupled estimate (1.6) in Winton et al. (2013). Accordingly, the meridional pattern of the feedbacks due to the active OHU is likewise distinct from those of the $slab_{4xCO_2}$ and $slab_{P-OHU}$ (Figures 4c–4g, compare dashed and solid red lines).

Analysis of the radiative feedback components shows that the shortwave (SW) clear-sky component is the primary cause of the large efficacy of the active ocean response. The reduced effective climate sensitivity, implied by λ_{A-OHU}, is due to the large SW clear-sky feedback offsetting the longwave (LW) clear-sky feedback effect. This result appears to be different from those of Trossman et al. (2016) and Rugenstein et al. (2016), which pointed to SW cloud feedback as the leading factor in mediating the atmospheric response to changes in ocean dynamics. Here because of the large cancellation between the LW and SW cloud components,
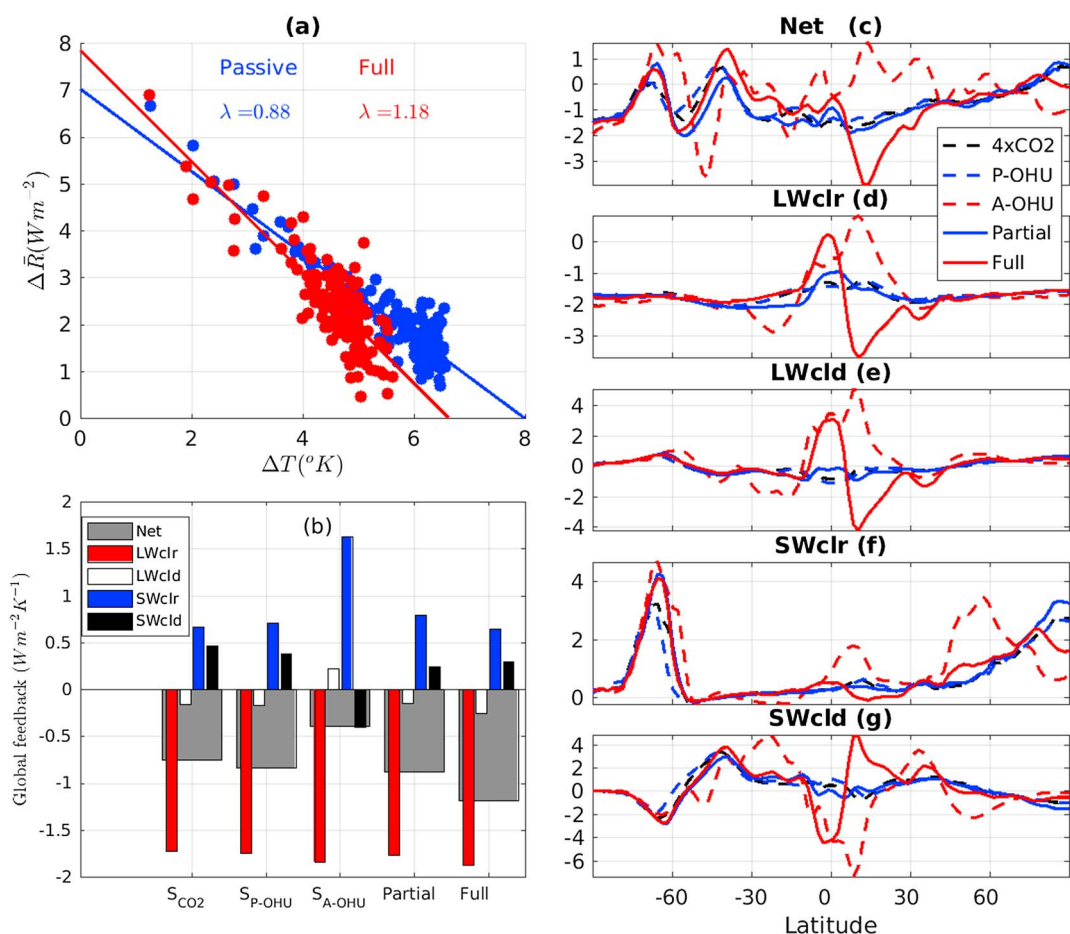
Figure 4. (a) Global climate feedback parameter (λ, W m^{-2} K^{-1}) in the partially coupled (passive component) (blue) and fully coupled (red) experiments. (b) Climate feedback components in the slab with only CO_2 forcing (Slab$_{CO2}$); with CO_2 and passive OHU forcing (slab$_{P-OHU}$), and with active OHU forcing only (slab$_{A-OHU}$); and in the partially coupled (partial) and fully coupled (full) experiments. (c) Meridional pattern of the global feedback parameter, and its components: (d) longwave clear sky, (e) longwave cloud, (f) shortwave clear sky, and (g) shortwave cloud.

they are not the primary cause of the large forcing efficacy in slab$_{A-OHU}$. Further inspection of the sea ice field indicates that the enhanced SW clear-sky feedback is the result of the increased sea ice associated with major cooling in the north Atlantic in slab$_{A-OHU}$ (compare the SSTs in Figure S6).

4. Summary and Discussion

In this study, we elucidate the role of ocean circulation changes in time-varying climate sensitivity by formulating a novel partially coupled framework using temperature-like passive tracers. We decompose ocean temperature anomaly and OHU into passive and active components, by comparing the response to CO_2 quadrupling in a partially coupled experiment, in which the impact of ocean circulation change on surface fluxes is disabled, to a fully coupled one. The passive component is attributable solely to atmospheric changes, while the active component is due to ocean circulation changes *and* its surface interactions. The ocean circulation-induced redistributive SST pattern, when uncoupled, includes NH subpolar cooling and tropical warming and causes a net global surface warming. Through coupling to the atmosphere, this redistributive pattern induces a slowly evolving active OHU pattern, characterized by tropical heat release and NH subpolar uptake, and a predominantly cool active SST pattern, which causes the weaker global surface warming in the fully coupled experiment. Further slab experiments reveal that the reduced effective climate sensitivity is due to the high efficacy of the active OHU; the effective sensitivity associated with the passive OHU is not significantly different from the equilibrium one. The high efficacy of the active OHU arises from the SW clear-sky feedback through an enhanced ice-snow albedo feedback in the NH high latitudes.

The passive and active ocean temperature components, as defined here, explain the fully coupled stationary and evolving SST, OHU, and radiative feedbacks patterns, and reduced effective climate sensitivity, because they completely isolate all ocean-driven changes. Prior surface-forced and redistributive ocean temperature decompositions (Banks & Gregory, 2006; Bouttes et al., 2014; Gregory et al., 2016; Marshall et al., 2015; Xie & Vallis, 2012) cannot isolate the stationary or evolving components, because they both contain ocean-driven changes. The active OHU has been isolated using other methods (redistribution feedback and redistributed heat) in Bouttes et al. (2014), Garuba and Klinger (2016), and Gregory et al. (2016). However, as noted in these studies, the active component is exaggerated (double counted) because their ocean circulation change is forced by fully coupled derived fluxes or target SST, which already includes an ocean-driven component. The partial coupling method here avoids this overestimation, by allowing the ocean model to be forced only with the CO_2-induced surface heat fluxes. Additionally, the uncoupled ocean redistributive component here isolates more cleanly the ocean-only effect, unlike ocean-only simulations forced with fully coupled surface fluxes, and shows that the net global surface cooling and deeper uptake in the fully coupled response is a coupled effect, not an ocean-only effect, as previously suggested in ocean-only studies (Garuba & Klinger, 2016; Xie & Vallis, 2012). This result underlines the need for caution in the interpretation of ocean-only experiments forced by fully coupled derived surface fluxes, as it may include a coupled effect.

The fully coupled pattern is often thought to be evolving toward a more subpolar pattern with time (Rose et al., 2014; Winton et al., 2013), but our results here suggest that this is only true for the NH subpolar region; the subpolar uptake in the Southern Ocean is passive and stationary during the time frame examined. The NH subpolar region is also the primary contributor to the high efficacy of the OHU here, due primarily to the ice-albedo feedback magnifying the active response in this area. The SH subpolar uptake pattern contributes little to the radiative feedback pattern change in the fully coupled response. Interestingly, the fully coupled surface air temperature evolving pattern here resembles the multimodel one, in the study of Andrews et al. (2015). The result here, therefore, offers a direct verification that the evolving OHU and SST patterns in the fully coupled response are indeed caused by ocean circulation changes, as previously suggested (Andrews et al., 2015; Armour et al., 2013; Haugstad et al., 2017; Rose et al., 2014; Rugenstein et al., 2016).

We show that the active OHU component is the main reason for the reduced effective climate sensitivity. As the ocean continues its course to equilibration, we suspect the active OHU will gradually diminish with time, as the effective climate sensitivity gradually increases (i.e., the red slope in Figure 4a becomes gentler with time), while the passive OHU pattern will remain roughly fixed and contribute little to the climate sensitivity increase during this slow adjustment period. The larger contribution of the SW clear-sky feedback to the high efficacy of the active OHU here is different from the previous studies suggesting the importance of cloud feedbacks (Andrews et al., 2015; Rose & Rayborn, 2016; Rugenstein et al., 2016; Trossman et al., 2016). The large magnitude of the SW clear-sky feedback in slab$_{A-OHU}$ is, undoubtedly, influenced by nonlinearities in the ice-albedo feedback due to lack of CO_2 induced warming in this experiment; nevertheless, the SW clear-sky feedback is also the largest change between the partially and fully coupled experiments both of which have increase in CO_2.

However, we note that sea ice is not considered in the aqua-planet studies of Rose et al. (2014); furthermore, the clear-sky SW feedback associated with idealized high-latitude OHU with active sea ice in Rugenstein et al. (2016) also accounts for most of the reduction of the net feedback and the clear-sky SW feedback. Our result here suggests that there is a physical basis for the SW clear-sky component dominance. Finally, we point out that the passive and active decomposition, and the relative importance of the SW clear-sky and cloud radiative feedbacks components will vary with different models. Further studies with several models will be needed to demonstrate the robustness of relative importance of the passive/active response and clear-sky/cloud radiative components in effective climate sensitivity.

References

Andrews, T., Gregory, J. M., & Webb, M. J. (2015). The dependence of radiative forcing and feedback on evolving patterns of surface temperature change in climate models. *Journal of Climate*, *28*(4), 1630–1648. https://doi.org/10.1175/JCLI-D-14-00545.1

Armour, K. C., Bitz, C. M., & Roe, G. H. (2013). Time-varying climate sensitivity from regional feedbacks. *Journal of Climate*, *26*(13), 4518–4534.

Armour, K. C., Marshall, J., Scott, J. R., Donohoe, A., & Newsom, E. R. (2016). Southern ocean warming delayed by circumpolar upwelling and equatorward transport. *Nature Geoscience*, *9*(7), 549–554.

Banks, H. T., & Gregory, J. M. (2006). Mechanisms of ocean heat uptake in a coupled climate model and the implications for tracer based predictions of ocean heat uptake. *Geophysical Research Letters*, *33*, L07608. https://doi.org/10.1029/2005GL025352

Bitz, C. M., Shell, K., Gent, P., Bailey, D., Danabasoglu, G., Armour, K., ... Kiehl, J. (2012). Climate sensitivity of the Community Climate System Model, version 4. *Journal of Climate*, *25*(9), 3053–3070.

Bouttes, N., Gregory, J., Kuhlbrodt, T., & Smith, R. (2014). The drivers of projected North Atlantic sea level change. *Climate Dynamics*, *43*(5–6), 1531–1544.

Danabasoglu, G., & Gent, P. R. (2009). Equilibrium climate sensitivity: Is it accurate to use a slab ocean model? *Journal of Climate*, *22*(9), 2494–2499. https://doi.org/10.1175/2008JCLI2596.1

Danabasoglu, G., Bates, S. C., Briegleb, B. P., Jayne, S. R., Jochum, M., Large, W. G., ... Yeager, S. G. (2012). The CCSM4 ocean component. *Journal of Climate*, *25*(5), 1361–1389.

Garuba, O. A., & Klinger, B. (2016). Ocean heat uptake and interbasin transport of the passive and redistributive components of surface heating. *Journal of Climate*, *29*(20), 7507–7527. https://doi.org/10.1175/JCLI-D-16-0138.1.

Geoffroy, O., Saint-Martin, D., Bellon, G., Voldoire, A., Olivié, D. J. L., & Tytéca, S. (2013). Transient climate response in a two-layer energy-balance model. Part II: Representation of the efficacy of deep-ocean heat uptake and validation for CMIP5 AOGCMs. *Journal of Climate*, *26*(6), 1859–1876. https://doi.org/10.1175/JCLI-D-12-00196.1

Gregory, J., Ingram, W., Palmer, M., Jones, G., Stott, P., Thorpe, R., ... Williams, K. (2004). A new method for diagnosing radiative forcing and climate sensitivity. *Geophysical Research Letters*, *31*, L03205. https://doi.org/10.1029/2003GL018747

Gregory, J. M., Bouttes, N., Griffies, S. M., Haak, H., Hurlin, W. J., Jungclaus, J., ... Winton, M. (2016). The Flux-Anomaly-Forced Model Intercomparison Project (FAFMIP) contribution to CMIP6: Investigation of sea-level and ocean climate change in response to CO_2 forcing. *Geoscientific Model Development*, *9*(11), 3993–4017. https://doi.org/10.5194/gmd-9-3993-2016

Haugstad, A., Armour, K., Battisti, D., & Rose, B. (2017). Relative roles of surface temperature and climate forcing patterns in the inconstancy of radiative feedbacks. *Geophysical Research Letters*, *44*, 7455–7463. https://doi.org/10.1002/2017GL074372

Held, I. M., Winton, M., Takahashi, K., Delworth, T., Zeng, F., & Vallis, G. K. (2010). Probing the fast and slow components of global warming by returning abruptly to preindustrial forcing. *Journal of Climate*, *23*(9), 2418–2427. https://doi.org/10.1175/2009JCLI3466.1

Hunke, E. C., Lipscomb, W. H., Turner, A. K., Jeffery, N., & Elliott, S. (2010). CICE: The Los Alamos sea ice model documentation and software user's manual version 4.1 LA-CC-06-012 (p. 675). T-3 Fluid Dynamics Group, Los Alamos National Laboratory.

Luo, Y., Lu, J., Liu, F., & Garuba, O. (2016). The role of ocean dynamical thermostat in delaying the El Niño-like response over the equatorial pacific to climate warming. *Journal of Climate*, *30*(8), 2811–2827.

Marshall, J., Scott, J. R., Armour, K. C., Campin, J. M., Kelley, M., & Romanou, A. (2015). Ocean's role in the transient response of the climate to abrupt greenhouse gas forcing. *Climate Dynamics*, *44*(7–8), 2287–2299.

Murphy, J. (1995). Transient response of the Hadley Centre coupled ocean-atmosphere model to increasing carbon dioxide. Part III: Analysis of global-mean response using simple models. *Journal of Climate*, *8*(3), 496–514.

Neale, R. B., Chen, C.-C., Gettelman, A., Lauritzen, P. H., Park, S., Williamson, D. L., ... Taylor, M. A. (2012). Description of the NCAR Community Atmosphere Model (CAM 5.0) (NCAR Tech. Note NCAR/TN-486+ STR). Boulder, CO: National Centre for Atmosphere Research.

Oleson, K. W., Lawrence, D. M., Gordon, B., Flanner, M. G., Kluzek, E., ... Feddema, J. (2010). Technical description of version 4.0 of the Community Land Model (CLM) (NCAR/TN-478+STR). Boulder, CO: National Centre for Atmosphere Research.

Rose, B. E., Armour, K. C., Battisti, D. S., Feldl, N., & Koll, D. D. (2014). The dependence of transient climate sensitivity and radiative feedbacks on the spatial pattern of ocean heat uptake. *Geophysical Research Letters*, *41*, 1071–1078. https://doi.org/10.1002/2013GL058955

Rose, B. E., & Rayborn, L. (2016). The effects of ocean heat uptake on transient climate sensitivity. *Current Climate Change Reports*, *2*(4), 190–201.

Rugenstein, M. A. A., Caldeira, K., & Knutti, R. (2016). Dependence of global radiative feedbacks on evolving patterns of surface heat fluxes. *Geophysical Research Letters*, *43*, 9877–9885. https://doi.org/10.1002/2016GL070907

Senior, C. A., & Mitchell, J. F. (2000). The time-dependence of climate sensitivity. *Geophysical Research Letters*, *27*(17), 2685–2688.

Trossman, D. S., Palter, J. B., Merlis, T. M., Huang, Y., & Xia, Y. (2016). Large-scale ocean circulation-cloud interactions reduce the pace of transient climate change. *Geophysical Research Letters*, *43*, 3935–3943. https://doi.org/10.1002/2016GL067931

Williams, K., Ingram, W., & Gregory, J. (2008). Time variation of effective climate sensitivity in GCMs. *Journal of Climate*, *21*(19), 5076–5090.

Winton, M., Griffies, S. M., Samuels, B. L., Sarmiento, J. L., & Frölicher, T. L. (2013). Connecting changing ocean circulation with changing climate. *Journal of climate*, *26*(7), 2268–2278.

Winton, M., Takahashi, K., & Held, I. M. (2010). Importance of ocean heat uptake efficacy to transient climate change. *Journal of Climate*, *23*(9), 2333–2344.

Xie, P., & Vallis, G. K. (2012). The passive and active nature of ocean heat uptake in idealized climate change experiments. *Climate Dynamics*, *38*(3–4), 667–684. https://doi.org/10.1007/s00382-011-1063-8